Clinical Radiology 74 (2019) 896.e1–896.e8

Contents lists available at ScienceDirect

Clinical Radiology

journal homepage: www.clinicalradiologyonline.net

Prediction of prostate cancer aggressiveness with a combination of radiomics and machine learning-based analysis of dynamic contrast-enhanced MRI

B. Liu [a], J. Cheng [b], D.J. Guo [a], X.J. He [a], Y.D. Luo [a], Y. Zeng [c,**], C.M. Li [a,*]

[a] *Department of Radiology, The Second Affiliated Hospital of Chongqing Medical University, No. 76, Linjiang Road, Yuzhong District, Chongqing, 400000, China*

[b] *Basic Medical College of Chongqing Medical University, No. 1 Medical School Road, Yuzhong District, Chongqing, 400042, China*

[c] *Department of Radiology, The Third Affiliated Hospital of Chongqing Medical University, No. 1 Shuanghu Branch Road, Yubei District, Chongqing, 401120, China*

ARTICLE INFORMATION

Article history:
Received 9 February 2019
Accepted 16 July 2019

AIM: To investigate whether the combination of radiomics and automatic machine learning-based classification of original images from multiphase dynamic contrast-enhanced (DCE)-magnetic resonance imaging (MRI) can predict prostate cancer (PCa) aggressiveness before biopsy.

MATERIALS AND METHODS: Forty consecutive biopsy-confirmed PCa patients were included. Biopsy was performed within 4 weeks after the DCE-MRI examinations. According to the time–signal-intensity curve, lesion segmentation was performed on the first and on the strongest phase of the enhancement on the original DCE-MRI images, and 1,029 quantitative radiomics features were calculated automatically from each lesion, wherein there were three datasets available (Dataset-F, Dataset-S and Dataset-FS). The variance threshold method, select k-best method and least absolute shrinkage and selection operator (LASSO) algorithm were used to reduce the feature dimensions. Five machine learning approaches leveraging cross-validation were employed, and the clinical value of each model was evaluated by area under the receiver operating characteristic curve (AUC). Correlation analysis was performed between the features of the machine learning model that achieved the best classification performance and the Gleason score (GS) of the PCa lesion.

RESULTS: Eight, four, and 16 features were selected as optimal subsets in Dataset-F, -S and -FS, respectively. Among all three datasets, logistic regression (LR)-based analysis with Dataset-FS had the highest predication efficacy (AUC=0.93). Ten features in Dataset-FS showed

* Guarantor and correspondent: C. Li, Department of Radiology, The Second Affiliated Hospital of Chongqing Medical University, No. 76, Linjiang Road, Yuzhong District, Chongqing, China. Tel.: +8613618302013.

** Guarantor and correspondent: Y. Zeng, Department of Radiology, The Third Affiliated Hospital of Chongqing Medical University, No. 1 Shuanghu Branch Road, Yubei District, Chongqing, China. Tel.: +8613452122792.

E-mail addresses: 1294583212@qq.com (Y. Zeng), li_chuanming@yeah.net (C.M. Li).

https://doi.org/10.1016/j.crad.2019.07.011

significantly positively correlation with GS. The model performance of Dataset-F was generally better than that in Dataset-S.

CONCLUSIONS: A combination of radiomics and machine learning-analysis based analysis of the union of the first and strongest phases of original DCE-MRI images can predict PCa aggressiveness non-invasively, accurately, and automatically.

Introduction

Globally, prostate cancer (PCa) is the second most common type of cancer and the fifth leading cause of cancer-related death in men.[1] It is the most common cancer in males in 84 countries, occurring more commonly in the developed world, and rates of PCa have been increasing in the developing world. In 2012, PCa occurred in 1.1 million men and caused 307,000 deaths, leading to deep suffering and a heavy burden to patients and society.[1] Most PCas are slow growing; however, some grow relatively quickly. Assessing the aggressiveness of PCa as early as possible has a dramatic impact on disease management, treatment choice, and patient prognosis.[2,3] Patients diagnosed with low-grade (LG) or intermediate-grade (IG) cancers may be treated with conservative management approaches such as active surveillance, while patients with high-grade (HG) cancers must undergo more radical strategies such as radiation therapy or surgery.[2] In addition, patients with low/intermediate invasiveness have better 5- and 10-year survival rates than do patients with high invasiveness.[3]

Until now, pathological biopsy has been regarded as the reference standard for evaluating PCa invasiveness; however, it has several accompanying risks of complications, such as infection/sepsis, haematuria, haematospermia, and rectal bleeding, which cause afflictions and anxiety among patients.[4] The prostate-specific antigen (PSA) level is a non-invasive method to evaluate the aggressiveness of PCa, but this test has very low specificity and accuracy.[5] In recent years, multiparametric (Mp) magnetic resonance imaging (MRI) has been regarded as a promising non-invasive tool for PCa detection or classification. Dynamic contrast-enhanced (DCE) MRI is one of the most widely used techniques in clinical work.[6] The tumour transfer constant (k^{trans}) value was found differed significantly between higher and lower-grade PCa tumours[6]; however, there is a large amount of overlap between two groups, and the clinical application of them is limited greatly, especially in the transition zone (TZ).

Radiomics is an innovative technology using data characterisation algorithms. It utilises an automated high-throughput extraction of a vast (200+) number of quantitative features from medical images, excavating latent data that were invisible to vision.[7–9] These distinctive imaging features may be useful for predicting prognosis and therapeutic response thus providing valuable information for personalised therapy. Machine learning is a field of artificial intelligence that uses statistical techniques to give computer systems the ability to "learn" from data to improve performance on a specific task without being explicitly programmed. The combination of artificial intelligence and radiomics can help distinguish benign from malignant lesions, predict lesion invasiveness, or therapeutic effect, and detect the relationship between medical images with gene signatures by analysing these high-throughput features.[10–12] Previously, it has been reported that sentinel lymph node metastasis of breast cancer could be accurately predicted using diffusion-weighted imaging (DWI) and T2-weighted imaging (T2WI) derived radiomics features.[10] Zhou *et al.*[11] illustrated that radiomics features indexed by the mean and grey-level run-length non-uniformity based on arterial phase images of the liver can predict biological invasiveness and the histological grading of hepatocellular carcinoma. For gliomas, texture and histogram features from Mp-MRI images and support vector machine (SVM) have also been proved great value in the classification of low-grade glioma and high-grade glioma.[12]

For prostatic carcinoma, Gleason grading is a well-validated factor and is regarded as the reference standard for aggressiveness evaluation.[13] The majority of patients with treatable/treated cancers have a GS of 6–7, and tumours with a GS of 8–10 tend to be advanced neoplasms that are unlikely to be cured.[14] Patients with a GS $\leq$7 have better biochemical disease-free survival and lower PCa-specific mortality than do patients with a GS $\geq$8.[14, 15] The present study investigated the clinical value of combining radiomics and automatic machine learning of original multiphase DCE-MRI images for discriminating PCas with low/intermediate or high invasive potential (GS $\leq$7 versus GS $\geq$8) before biopsy.

Materials and methods

This retrospective study was approved by the medical ethics committee of our hospital, and all patients provided informed consent.

Patient cohort

Between 1 January 2016 and 31 May 2018, 50 consecutive pathology confirmed PCa patients with Prostate Imaging-Reporting and Data System version 2 (PI-RADS v2) score of 4 or 5 were included. All of these patients had no contraindications for MRI and underwent MRI examinations with a 1.5-T MRI system (Signa Excite II, GE

Healthcare, Fairfield, CT, USA). Biopsy was performed within 4 weeks after the DCE-MRI examinations. Patients with poor MRI image quality of serious image artefact (n=2), those whose cancer location required a urethral catheter, those who had multiple lesions with different GSs (n=3), and those who had received prior treatment for PCa (i.e., hormonal therapy or transurethral resection of the prostate [TURP], n=5) were excluded from the analysis. Finally, 40 lesions from 40 patients were included in the study. Fig 1 details the patient selection process with a flow chart. Table 1 exhibits the demographic and histopathological characteristics of the patient cohort.

MRI acquisition

All of the patients underwent routine T1WI, fat-saturated respiratory-triggered fast recovery fast spin-echo (FRFSE) T2WI, echo planar imaging (EPI) DWI and DCE gradient-echo T1WI in axial planes. The full Mp-MRI parameters are listed in Table 2. For DCE-MRI, after the third dynamic scan, gadolinium (Gd3+; 0.1 mmol/kg; Omniscan GE Healthcare Life Sciences) was administered intravenously at a rate of 2.5 ml/s with an automatic power injector (Spectris MR Injector System; Medrad, Fairfield, CT, USA) followed by a 20 ml saline solution flush. During each phase of DCE-MRI 52 sections were scanned, and a total of 32 periods of uninterrupted scanning were performed. The scanning time was 313 seconds.

Histopathology and image segmentation

All 40 tumour lesion GSs were confirmed on samples from transperineal ultrasound-guided template saturation biopsy (24 core). Tumour locations on Mp-MRI images that matched the biopsy were identified by four observers by consensus: two radiologists (with 10 and 20 years of experience with Mp-MRI interpretation), one histopathologist (with 9 years of experience in pathological grading of malignant tumours), and one clinical urologist (with 5 years of experience in the diagnosis of urinary and reproductive neoplasms).

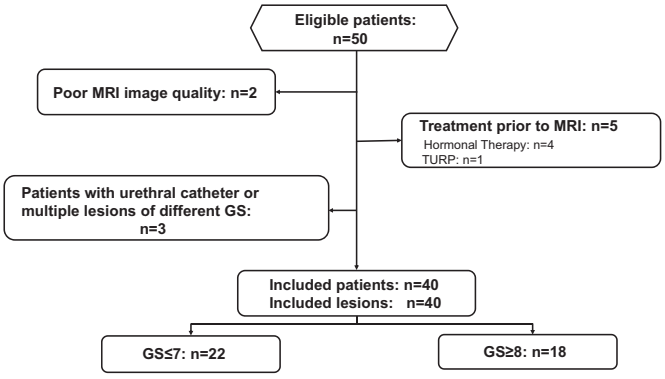

Figure 1 Flow chart of inclusion and exclusion criteria for patients and tumours. GS, Gleason score; TURP, transurethral resection of the prostate.

Table 1
Demographic and histopathological characteristics of the patient cohort

	n [range]
Number of patients	40
Number of lesions	40
Mean age	73 [59-93]
Mean PSA ng/ml	11.6 [0.4–25]
Gleason score, n (%)	
≤7	22 (55%)
3+3	5 (12%)
3+4	7 (18%)
4+3	10 (25%)
≥8	18 (45%)
4+4	11 (28%)
4+5	4 (9%)
5+3	3 (8%)
Tumour location, n (%)	
PZ	30 (75%)
TZ	10 (25%)

PSA, serum prostate specific antigen; PZ, peripheral zone; TZ, transition zone.

Time–signal-intensity curves of tumour lesions from DCE-MRI images were calculated using an advanced workstation from General Electric Medical Systems. According to the curve, regions of interest (ROIs) were delineated slice by slice on the whole tumour during the first phase of enhancement and during the strongest phase on axial DCE-MRI images. ROIs were outlined manually by radiologists who were blinded to the GSs of the patients, and all contours were reviewed by the senior radiologists. If there is a discrepancy, the senior radiologist decided on the tumour borders.[7] Finally, 40 ROIs from the first enhancement phase (Dataset-F), 40 ROIs from the strongest enhancement phase (Dataset-S), and 80 ROIs from both the first and strongest enhancement phase (Dataset-FS) were obtained. This process was performed using an open-source software[16] (3D slicer version 4.8.1; at http://slicer.org/; Fig 2).

Feature extraction and reduction

A total of 1,029 quantitative imaging features were extracted automatically from each ROI; these features can be grouped into four categories. Category 1 features (first order statistics) quantitatively delineate the distribution of

Table 2
MRI sequence parameters used for the study

	T1W	T2W FRFSE	EPI DWI	DCE
Repetition time (ms)	600	2200	4050	3.9
Echo time (ms)	8.7	70.2	78,2	1.3
Flip angle (degrees)	n/a	n/a	n/a	15
Field of view (mm)	260×260	260×260	260×260	400×320
Section thickness (mm)	5.6	5.6	5.6	6
Section gap(mm)	1	1	1	−2
Fat saturation	No	Yes	Yes	Yes
Base matrix	320×192	320×192	128×128	224×160
b-Values(s.mm^{-2})	n/a	n/a	0,1000	n/a
Number of excitations	2	4	4	0.73

T1W, T1-weighted; T2W FRFES, T2-weighted fat-saturated respiratory-triggered fast recovery fast spin-echo; EPI DWI, echo planar imaging diffusion-weighted imaging; DCE, dynamic contrast-enhanced T1-weighted gradient-echo images.

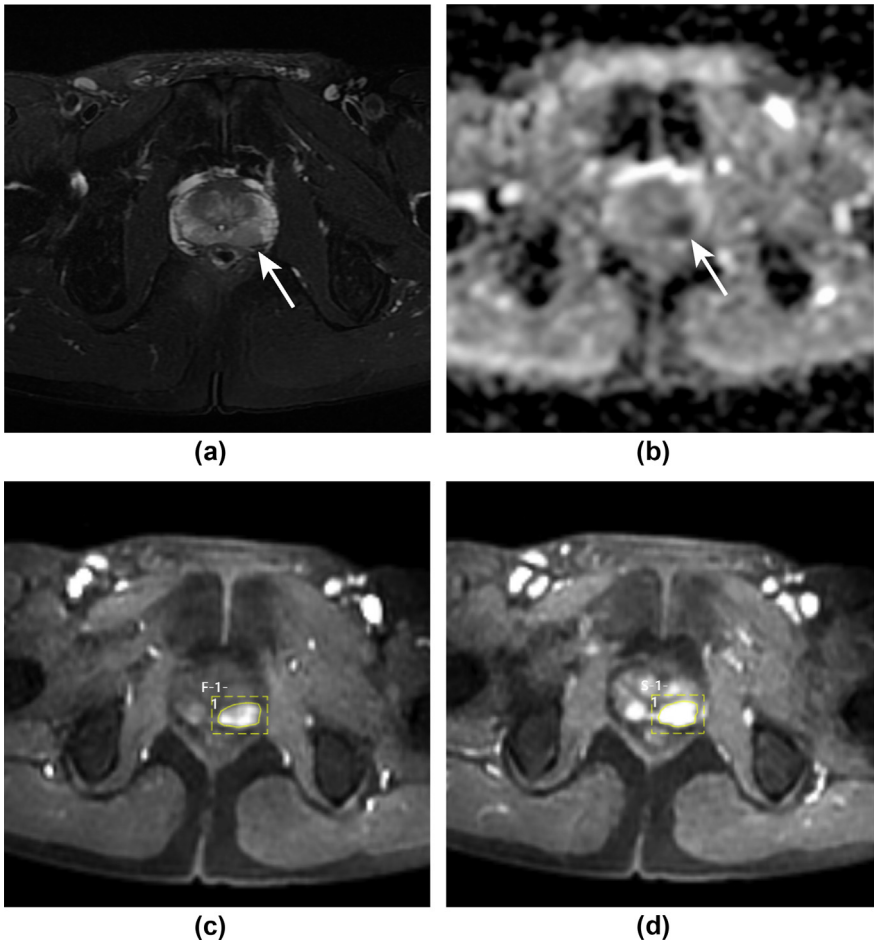

Figure 2 A 61-year-old man with a tumour of GS 6 (3+3) in the left peripheral zone. (a) Tumour lesion on T2-weighted image (arrow). (b) Tumour lesion on apparent diffusion coefficient (ADC) map (arrow). (c) Tumour lesion contoured on the first phase of enhancement (F-1-1). (d) Tumour lesion contoured on the strongest phase of enhancement (S-1-1).

voxel intensities within the MRI images through commonly used and basic metrics. Category 2 features (shape- and size-based features) reflect the shape and size of the regions. Textural features calculated from the grey-level run-length matrix (glrlm), grey-level size zone matrix (glszm) and grey-level co-occurrence matrix (glcm) quantify differences in the heterogeneity of regions and are classified as category 3 (texture features). Finally, category 4 (higher order statistics features) includes intensity and texture features derived from image transformation of the original image (filters of the image transformation are as follows: exponential, square, square root, logarithm, and wavelet). The mathematical expressions and semantic meanings of the features used in the present study can be found at http://pyradiomics.readthedocs.io/en/latest/features.html#module-radiomics.

Feature reduction is a procedure of selecting a truly worthwhile subset of features for the predictive model. Relatively insignificant features may contribute little to the model and actually decrease the predictive performance. Firstly, a threshold of 0.8 was used to retain all eigenvalues with a variance greater than 0.8 for further analysis. Thereafter, the chi-square test was used to measure the relationship between features and classification result (GS $\leq$7 versus GS $\geq$8), and features with p-values $<$0.05 were selected for the next step investigation. Finally, L1 regularisation to add the L1 norm of the linear model coefficient to the loss function as a penalty term was utilised so that the coefficient corresponding to the weak correlation feature became 0, and feature selection was realised. This approach is called the least absolute shrinkage and selection operator (LASSO) algorithm and has favourable performance for filtering features and reducing the complexity of the model.[17] The above procedure was repeated for each dataset to select the optimal subset for the machine learning model.

Model construction and evaluation

Before building the machine learning model, the input eigenvalues were firstly normalised: the mean was removed and scaled to the unit variance.[18] For the three datasets (Dataset-F, Dataset-S and Dataset-FS), five supervised machine learning methods leveraging stratified (K=5)-fold cross-validation were employed. The machine learning methods were as follows: SVM based on linear kernel, logistic regression (LR), random forests (RF), decision tree (DT)

and k-nearest neighbour (KNN). These approaches were utilised because of their practicability, simplicity, and experimental efficacy in the literature.[18–20] In the present study, each machine learning method was trained and validated independently using the stratified (K=5)-fold cross-validation approach to estimate the generalisation ability of the classifier. Cross-validation can assess how the results of a model will generalise to an independent data set.[21]

Statistical analysis

The accuracy, sensitivity, specificity, and area under the receiver operating characteristic (ROC) curve (AUC) were used to evaluate the performance of each machine learning model for the classification tasks. Moreover, correlation analysis was performed between features of the machine learning approaches yielding the highest classification generalisation ability and GSs of the lesions. Firstly, the feature values were checked with the one-sample Kolmogorov–Smirnov test for normality. Then, the correlation between the values and GSs was evaluated through Pearson's correlation test for data fitting the normal distribution or Spearman rank correlation analysis for data violating the normal distribution. $p<0.05$ were regarded as statistically significant. Feature extraction, reduction and model construction were performed on R software, which is a free and open-source tool.[22] SPSS (version 17.0) was used for the correlation tests.

Results

Feature dimension reduction and optimal subset selection

In Dataset-F, 617 features from 1,029 features were selected using the variance threshold method. Then, with the select k-best method, 89 features were selected. Finally, eight features were selected as an optimal subset with the LASSO algorithm. By repeating the above procedure, four and 16 signatures were selected as the optimal subset among Dataset-S and Dataset-FS, respectively. All these features are demonstrated in Fig 3.

Evaluation of classifiers performance

In Dataset-F, KNN yielded the best predict efficacy (AUC=0.88; accuracy=0.85) for the classification of PCas with low/intermediate and high invasive. In Dataset-S, LR generated the best performance (AUC=0.84; accuracy=0.76), while in Dataset-FS, LR was also the best classifier (AUC=0.93; accuracy=0.90). Among all the classifiers, LR trained with Dataset-FS had the best performance compared with the others (Table 3).

Correlation between radiomics features of Dataset-FS and GS

According to the evaluation of classifier performance, the radiomics features of Dataset-FS offered the highest predicative efficacy. Sixteen optimal features were obtained in the Dataset-FS. Ten features of them (F-least axis shape, S-least axis shape, F-total energy first-order statistics, F total energy logarithm, S-large area emphasis (LAE) in glszm-wavelet-LLH, S-large area high grey-level emphasis (LAHGLE) in glszm texture features, F-zone entropy (ZE) in glszm-wavelet-HHL, F-long run emphasis (LRE) in glrlm-wavelet-HHH, F-run length non-uniformity (RLN) in glrlm-exponential and S-LRE in glrlm wavelet HHH) were found significantly correlated ($p<0.05$) with the GS of the lesions (Table 4).

Discussion

Assessing PCa invasiveness as early as possible is essential for disease management, treatment choice, and patient prognosis. Pathological biopsy, PSA level and Mp-MRI are popular tools for estimation of PCa invasiveness, but they all have various complications that limit their clinical use. It is extremely urgent to explore a new non-invasive method with high accuracy. Radiomics leveraging data characterisation algorithms can automatically extract a large number high-throughput quantitative features from original medical images and can offer additional information that is far beyond the scope of visual analysis. Furthermore, proper feature dimensionality reduction and machine learning approaches can help get the optimal features and achieve an efficient and robust classification. The combination of these techniques is very valuable and can help clinicians determine the appropriate treatment for their patients without unnecessary interventions. In clinical work, the combination of radiomics features derived from original multiphase DCE-MRI with machine learning to predict the aggressiveness of PCa has not been reported.

The present study found that LR based on Dataset-FS, which employed the integration of the first and the strongest enhanced phases of DCE-MRI, showed the best classification efficacy compared with the other models. This method can facilitate the diagnostic ability to predict PCa invasiveness with an accuracy of 0.90 with no complications of infection/sepsis, haematuria, haematospermia, or rectal bleeding. It is a valuable means to help clinicians determine the appropriate treatment for their patients and has wide applicability in clinical practice. Previously, Rozenberg *et al.*[23] combined ADC-derived features and LR to predict the aggressiveness of PCa with an accuracy of 0.75. Another study integrating features based on pharmacokinetic model parameter maps and SVM had an accuracy of 0.77 for detecting neoplasms in the peripheral zone (PZ).[24]

Radiomics features can clearly reveal tiny changes in the histological anatomy and pathophysiology of neoplasms that are hard to identify quantitatively with the naked eye and are often overlooked in clinical practice. In this study, 16 features were selected as an optimal subset in Dataset-FS, and 10 of these features showed close correlation with GS of the lesions. These findings indicate that these features are characteristic of PCa and could reflect the invasive nature of it. Among all 10 features, there was one first-order statistics

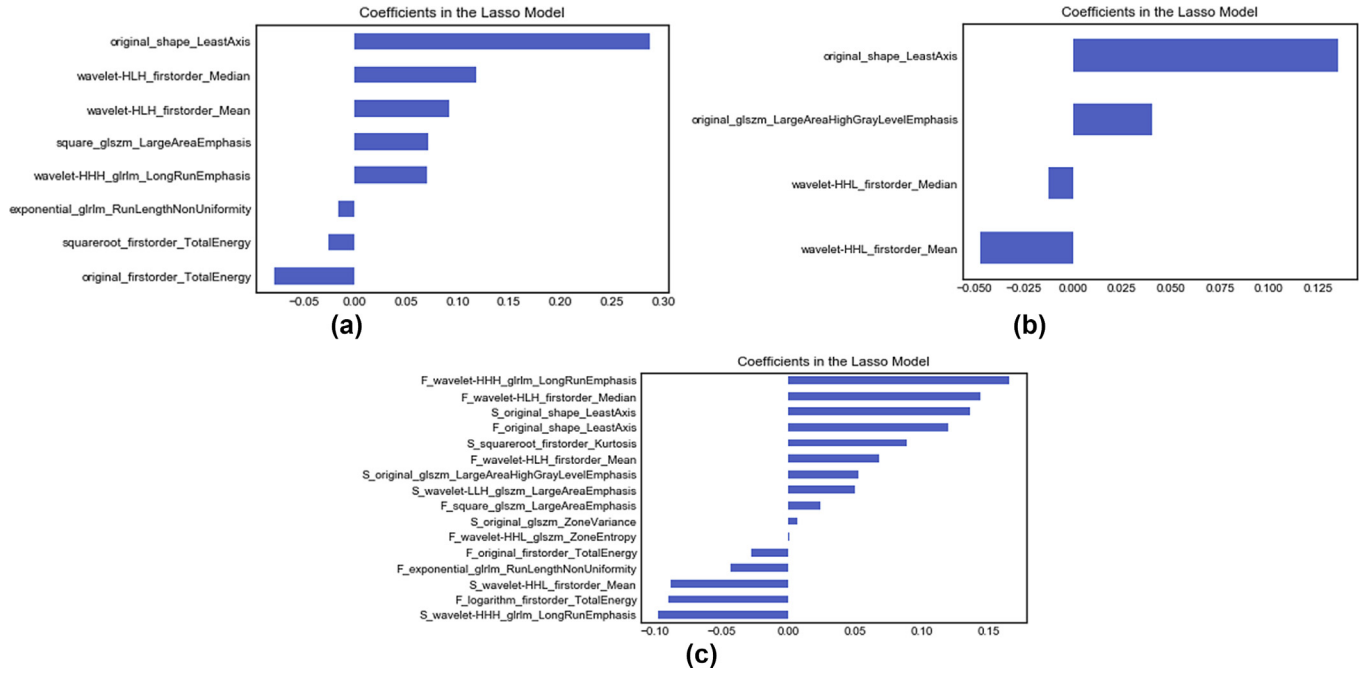

Figure 3 Radiomics features in the optimal subsets. (a) Optimal subset of Dataset-F. (b) Optimal subset of Dataset-S. (c) Optimal subset of Dataset-FS. Wherein the absolute value of the coefficients from the LASSO model only represents the contribution of each feature in each dataset. L: low-pass filter; H: high-pass filter; glszm: grey-level size zone matrix; glrlm: grey-level run-length matrix; LASSO: least absolute shrinkage and selection operator.

feature, two shape- and size-based features, one texture feature, and six higher-order statistics features. The F-least axis shape, S-least axis shape, F-total energy first-order statistics, and F-total energy logarithm are indices of tumour volume and signal intensity. PCa with high invasive potential had a larger volume and more powerful signal intensity on the enhanced scans than neoplasms with low/intermediate invasive potential. The possible reason is that HG-PCa has a greater requirement for neovascularisation and uptakes more contrast agent than LG/IG-PCa.[6,25] The

Table 3
Predictive performance of each classifier for each dataset

Dataset/machine	AUC (95% CI)	Accuracy	Sensitivity	Specificity
Dataset-F				
LR	0.87 (0.72–0.93)	0.83	0.77	0.89
RF	0.83 (0.60–0.82)	0.71	0.91	0.50
DT	0.71 (0.59–0.83)	0.71	0.64	0.78
KNN	0.88 (0.74–0.93)	0.85	0.91	0.78
SVM	0.84 (0.69–0.90)	0.80	0.77	0.83
Dataset-S				
LR	0.84 (0.65–0.86)	0.76	0.91	0.61
RF	0.80 (0.62–0.85)	0.75	0.82	0.67
DT	0.69 (0.58–0.81)	0.69	0.77	0.61
KNN	0.82 (0.74–0.93)	0.84	0.95	0.72
SVM	0.83 (0.65–0.86)	0.76	0.91	0.61
Dataset-FS				
LR[a]	0.93 (0.82–0.97)	0.90	0.86	0.94
RF	0.82 (0.65–0.87)	0.77	0.86	0.67
DT	0.77 (0.66–0.87)	0.77	0.86	0.67
KNN	0.91 (0.70–0.91)	0.82	0.91	0.72
SVM	0.90 (0.71–0.92)	0.82	0.86	0.78

AUC, area under the ROC curve; ROC, receiver operating characteristic curve; 95% CI, 95% confidence interval; LR, logistic regression; RF, random forests; DT, decision tree; KNN, k-nearest neighbour; SVM, support vector machine.
[a] Represents the classifier with the best performance among all of the models.

Table 4
Correlation tests between radiomics features of Dataset-FS and Gleason score

Dataset-feature-category or filter	Correlation coefficient	*p*-Value
F-least axis shape[a]	0.637	0.001
S-least axis shape[a]	0.636	0.001
F-total energy first-order statistics[a]	0.598	0.001
F-total energy logarithm[a]	0.570	0.001
S-large area emphasis in glszm-wavelet-LLH[a]	0.514	0.001
S-large area high grey level emphasis in glszm-texture features[a]	0.508	0.001
F-zone entropy in glszm-wavelet-HHL[a]	0.459	0.003
F-long run emphasis in glrlm-wavelet-HHH[a]	0.431	0.005
F-run length non-uniformity in glrlm-exponential[a]	0.350	0.027
S-long run emphasis in glrlm-wavelet-HHH[a]	0.336	0.034
F-large area emphasis in glszm-square	0.270	0.093
S-zone variance in glszm-texture features	0.264	0.100
F-median-wavelet-HLH	0.243	0.132
F-mean-wavelet-HLH	0.230	0.154
S-kurtosis square root	0.206	0.202
S-m,ean-wavelet-HHL	−0.209	0.195

[a] Represents significant correlation ($p<0.05$).

remaining six features (S-LAE in glszm-wavelet-LLH, S-LAHGLE in glszm-texture features, F-ZE in glszm-wavelet-HHL, F-LRE in glrlm-wavelet-HHH, F-RLN in glrlm-exponential and S-LRE in glrlm-wavelet-HHH) are indices of texture and heterogeneity. Increasing values of these features in HG-PCa indicate a coarser texture and increasing heterogeneity when compared with LG/IG-PCa. This result was strongly consistent with those of previous studies.[22, 26, 27] Among all the 10 features, most of them were higher-order statistics features and utilised wavelet transform. Higher-order statistics features could display subtle alterations in tissue morphology more explicitly.[28] Wavelet transform can eliminate noise in the image or sharpen the image, and this process does not alter the semantic meaning of the features.

In this study, DCE-MRI was used for radiomics analysis and machine learning, which provided images with high temporal resolution, high spatial resolution, high signal-to-noise ratio and enhanced tissue information regarding prostate.[29] Previously, radiomics analysis based of other MRI sequences have been reported.[30, 31] Chaddad *et al.*[30] combined RF with features derived from T2W and DWI to predict the PCa invasiveness with an AUC of 0.65. Shiradkar *et al.*[31] introduced a machine learning-based classifier of forecasting PCa biochemical recurrence by integrating T2W- and ADC-based radiomics features and obtained an AUC of 0.73; however, most of lesions on DWI and T2W images exhibit unclear or incomplete borders, which is unfavourable for segmenting the lesions completely. It is more accurate to overlay ROIs on DCE-MRI images. Previously, DCE-MRI-derived perfusion parameters, including the pharmacokinetic model parameters K^{trans} and K_{ep}, have offered the possibility of differentiating low-grade from medium-grade plus high-grade PCa with an AUC of 0.72.[25] Another study using 13 perfusion parameters with an SVM demonstrated an accuracy of 0.77 for PCa detection[24]; however, DCE pharmacokinetic analysis mostly indicates microcirculation function without information regarding the tissue morphological characteristics. Original DCE-MRI images could offer more information than colour maps of pharmacokinetic parameters. On the other hand, most studies using DCE pharmacokinetic images used no more than 20 image features. In this study, the lesions were overlaid slice by slice, and 1,029 radiomics features were employed to obtain comprehensive tissue information regarding the tumour, and a higher accuracy (0.90) was obtained.

DCE-MRI has many scanning phases, and until now, there is no consensus that which phase of feature extraction could offer the best prediction. Nie and colleagues found the third-phase enhanced scan could successfully predict the pathologic response of rectal cancer after preoperative chemoradiation therapy.[32] In breast cancer, Ming *et al.*[33] predicted the response of neoadjuvant chemotherapy using the first three phases of DCE-MRI. The strongest phase was also proved can reflect the invasiveness of tumours.[34] Therefore, in this study, we used the first and the strongest phases of tumour enhancement, which may have the greatest association with potential tissue information. The present observations showed that the model performance of Dataset-F was generally better than that of Dataset-S. The possible reason may be that the first phase of tumour enhancement has more diverse information than the strongest phase, which is in accordance with enhancement characteristics of PCa[35] (early-phase enhancement).

This study has several limitations. Firstly, because of the relatively small sample size, PZ and TZ neoplasms were not investigated separately. Secondly, most of the GSs were obtained through transperineal ultrasound-guided template saturation biopsy (24 core), which may differ from those obtained following radical prostatectomy. In the future work, the results will be confirmed with larger and more homogenised samples and PZ and TZ neoplasms will be analysed separately. Separate training and test and validation sets were not available in this study, but the fivefold cross-validation was employed, which may have similar effects. Finally, in the present study, radiomics of DCE-MRI with pathology results were compared directly, and not with conventional clinical interpretation. In the future work, radiomics of different imaging techniques including MRI, computed tomography (CT), positron-emission tomography (PET)-CT and other conventional clinical methods will be investigated regarding their clinical value.

In conclusion, the present study found that the DCE-MRI original image-derived radiomics features integrated with automatic machine learning approaches could predict PCa invasiveness non-invasively with high accuracy. Features extracted from the first phase of tumour enhancement have a stronger association with the pathophysiology of carcinoma than those extracted from the strongest phase. As a new technology, this method is independent of conventional clinical assessment. It may be an effective complement to conventional MRI and included in the new version of PI-RADS in the future.

Conflict of interest

The authors declare no conflict of interest.

Acknowledgements

The authors thank Huiyihuiying Medical Technology (Beijing) Co. Ltd, for their kind support. This work was supported by the National Key Research and Development Program of China (grant no. 2016YFC0107109) and the Medical Research Plan Project of Chongqing Health and Family Planning Commission (grant nos. 2016MSXM024; 2017MSXM035).

References

1. McGuire S. World cancer report 2014. Geneva, Switzerland: world Health organization, International agency for research on cancer, WHO press, 2015. *Adv Nutr* 2016 Mar 15;**7**(2):418–9.
2. Heidenreich A, Bastian PJ, Bellmunt J, *et al*. EAU guidelines on prostate cancer. part 1: screening, diagnosis, and local treatment with curative intent-update 2013. *Eur Urol* 2014;**65**(1):124–37.

3. Wright JL, Salinas CA, Lin DW, *et al*. Prostate cancer specific mortality and Gleason 7 disease differences in prostate cancer outcomes between cases with Gleason 4 + 3 and Gleason 3 + 4 tumours in a population based cohort. *J Urol* 2009;**182**(6):2702–7.
4. Bjurlin MA, Wysock JS, Taneja SS. Optimization of prostate biopsy: review of technique and complications. *Urol Clin North Am* 2014;**41**(2):299–313.
5. Lojanapiwat B, Anutrakulchai W, Chongruksut W, *et al*. Correlation and diagnostic performance of the prostate-specific antigen level with the diagnosis, aggressiveness, and bone metastasis of prostate cancer in clinical practice. *Prostate Int* 2014;**2**(3):133–9.
6. Hotker AM, Mazaheri Y, Aras O, *et al*. Assessment of prostate cancer aggressiveness by use of the combination of quantitative DWI and dynamic contrast-enhanced MRI. *AJR Am J Roentgenol* 2016;**206**(4):756–63.
7. Lambin P, Rios-Velazquez E, Leijenaar R, *et al*. Radiomics: extracting more information from medical images using advanced feature analysis. *Eur J Cancer* 2012;**48**(4):441–6.
8. Gillies RJ, Kinahan PE, Hricak H. Radiomics: images are more than pictures, they are data. *Radiology* 2016;**278**(2):563–77.
9. Ma W, Ji Y, Qi L, *et al*. Breast cancer Ki67 expression prediction by DCE-MRI radiomics features. *Clin Radiol* 2018;**73**(10):909 e901–5.
10. Dong Y, Feng Q, Yang W, *et al*. Preoperative prediction of sentinel lymph node metastasis in breast cancer based on radiomics of T2-weighted fat-suppression and diffusion-weighted MRI. *Eur Radiol* 2018;**28**(2):582–91.
11. Zhou W, Zhang L, Wang K, *et al*. Malignancy characterization of hepatocellular carcinomas based on texture analysis of contrast-enhanced MRI images. *J Magn Reson Imaging* 2017;**45**(5):1476–84.
12. Tian Q, Yan L-F, Zhang X, *et al*. Radiomics strategy for glioma grading using texture features from multiparametric MRI. *J Magn Reson Imaging* 2018 Dec;**48**(6):1518–28.
13. Kristiansen G, Egevad L, Amin M, *et al*. The 2014 consensus conference of the ISUP on Gleason grading of prostatic carcinoma. *Pathol* 2016;**37**(1):17–26.
14. Van Poppel H, Joniau S. An analysis of radical prostatectomy in advanced stage and high-grade prostate cancer. *Eur Urol* 2008;**53**(2):253–9.
15. Turker P, Bas E, Bozkurt S, *et al*. Presence of high grade tertiary Gleason pattern upgrades the Gleason sum score and is inversely associated with biochemical recurrence-free survival. *Urol Oncol* 2013;**31**(1):93–8.
16. Fedorov A, Beichel R, Kalpathy-Cramer J, *et al*. 3D slicer as an image computing platform for the quantitative imaging network. *Magn Reson Imaging* 2012;**30**(9):1323–41.
17. Feng ZZ, Yang X, Subedi S, *et al*. The LASSO and sparse least square regression methods for SNP selection in predicting quantitative traits. *IEEE/ACM Trans Comput Biol Bioinform* 2012;**9**(2):629–36.
18. Parmar C, Grossmann P, Bussink J, *et al*. Machine learning methods for quantitative radiomic biomarkers. *Sci Rep* 2015;**5**(1).
19. Vallieres M, Freeman CR, Skamene SR, *et al*. A radiomics model from joint FDG-PET and MRI texture features for the prediction of lung metastases in soft-tissue sarcomas of the extremities. *Phys Med Biol* 2015;**60**(14):5471–96.
20. Aerts HJ, Velazquez ER, Leijenaar RT, *et al*. Decoding tumour phenotype by noninvasive imaging using a quantitative radiomics approach. *Nat Comm* 2014;**5**:4006.
21. Guo W, Li H, Zhu Y, *et al*. Prediction of clinical phenotypes in invasive breast carcinomas from the integration of radiomics and genomics data. *J Med Imaging* 2015;**2**(4):041007.
22. Kolossvary M, Karady J, Szilveszter B, *et al*. Radiomic features are superior to conventional quantitative computed tomographic metrics to identify coronary plaques with napkin-ring sign. *Circ Cardiovasc Imaging* 2017 Dec;**10**(12):e006843.
23. Rozenberg R, Thornhill RE, Flood TA, *et al*. Whole-tumour quantitative apparent diffusion coefficient histogram and texture analysis to predict gleason score upgrading in intermediate-risk 3 + 4 = 7 prostate cancer. *AJR Am J Roentgenol* 2016;**206**(4):775–82.
24. Sung YS, Kwon HJ, Park BW, *et al*. Prostate cancer detection on dynamic contrast-enhanced MRI: computer-aided diagnosis versus single perfusion parameter maps. *AJR Am J Roentgenol* 2011;**197**(5):1122–9.
25. Vos EK, Litjens GJ, Kobus T, *et al*. Assessment of prostate cancer aggressiveness using dynamic contrast-enhanced magnetic resonance imaging at 3 T. *Eur Urol* 2013;**64**(3):448–55.
26. Bogowicz M, Riesterer O, Stark LS, *et al*. Comparison of PET and CT radiomics for prediction of local tumour control in head and neck squamous cell carcinoma. *Acta Oncol (Stockholm, Sweden)* 2017;**56**(11):1531–6.
27. Zhai TT, van Dijk LV, Huang BT, *et al*. Improving the prediction of overall survival for head and neck cancer patients using image biomarkers in combination with clinical parameters. *Radiother Oncol* 2017;**124**(2):256–62.
28. Huynh E, Coroller TP, Narayan V, *et al*. CT-based radiomic analysis of stereotactic body radiation therapy patients with lung cancer. *Radiother Oncol* 2016;**120**(2):258–66.
29. Hegde JV, Mulkern RV, Panych LP, *et al*. Multiparametric MRI of prostate cancer: an update on state-of-the-art techniques and their performance in detecting and localizing prostate cancer. *J Magn Reson Imaging* 2013;**37**(5):1035–54.
30. Chaddad A, Kucharczyk MJ. Multimodal radiomic features for the predicting Gleason score of prostate cancer. *Cancers (Basel)* 2018 Jul 28;**10**(8):E249.
31. Shiradkar R, Ghose S, Jambor I, *et al*. Radiomic features from pretreatment biparametric MRI predict prostate cancer biochemical recurrence: preliminary findings. *J Magn Reson Imaging* 2018 Dec;**48**(6):1626–36.
32. Nie K, Shi L, Chen Q, *et al*. Rectal cancer: assessment of neoadjuvant chemoradiation outcome based on radiomics of multiparametric MRI. *Clin Cancer Res* 2016;**22**(21):5256–64.
33. Fan M, Wu G, Cheng H, *et al*. Radiomic analysis of DCE-MRI for prediction of response to neoadjuvant chemotherapy in breast cancer patients. *Eur J Radiol* 2017;**94**:140–7.
34. Teruel JR, Heldahl MG, Goa PE, *et al*. Dynamic contrast-enhanced MRI texture analysis for pretreatment prediction of clinical and pathological response to neoadjuvant chemotherapy in patients with locally advanced breast cancer. *NMRI Biomed* 2014;**27**(8):887–96.
35. Weinreb JC, Barentsz JO, Choyke PL, *et al*. PI-RADS prostate imaging - reporting and data system: 2015, version 2. *Eur Urol* 2016;**69**(1):16–40.